Drug Design, Development and Therapy

Dovepress
open access to scientific and medical research

Open Access Full Text Article

ORIGINAL RESEARCH

Guanxinning Tablet Alleviates Post-Ischemic Stroke Injury Via Regulating Complement and Coagulation Cascades Pathway and Inflammatory Network Mobilization

Yule Wang[1], Yiran Li[2], Yue Zhou[2], Yue Gao[1], Lu Zhao[2]

[1]Zhejiang Key Laboratory of Traditional Chinese Medicine for the Prevention and Treatment of Senile Chronic Diseases, Department of Geriatrics, Affiliated Hangzhou First People's Hospital, School of Medicine, Westlake University, Hangzhou, People's Republic of China; [2]Pharmaceutical Informatics Institute, College of Pharmaceutical Sciences, Zhejiang University, Hangzhou, People's Republic of China

Correspondence: Lu Zhao; Yue Gao, Email lzhao@zju.edu.cn; gaoyue@hospital.westlake.edu.cn

Background: Currently, ischemic stroke (IS) continues to significantly contribute to functional deterioration and reduced life quality. Regrettably, the choice of neuro-rehabilitation interventions to enhance post-IS outcomes is limited. Guanxinning tablet (GXNT), a multi-component medicine composed of Danshen and Chuanxiong, has demonstrated neuroprotective potential against ischemic brain injury and diabetic encephalopathy. However, the therapeutic impact of GXNT on post-IS functional outcomes and pathological injury, as well as the underlying molecular mechanisms and anti-IS active substances, remain unclear.

Methods: To answer the above questions, neurological and behavioral assessment, cerebral lesions, and blood-brain barrier (BBB) integrity were combined to comprehensively investigate GXNT's pharmacodynamic effects against post-IS injury. The possible molecular mechanisms were revealed through transcriptome sequencing coupled with experimental verification. Furthermore, the brain tissue distribution of main components in GXNT, behavioral changes of IS zebrafish, and molecular docking were integrated to identify the anti-IS active compounds.

Results: Treatment with GXNT significantly mitigated the functional deficits, cerebral cortex lesions, and BBB disruption following IS. Transcriptome sequencing and bioinformatics analysis suggested that complement and coagulation cascades as well as inflammation might play crucial roles in the GXNT's therapeutic effects. Molecular biology experiments indicated that GXNT administration effectively normalized the abnormal expression of mRNA and protein levels of key targets related to complement and coagulation cascades (eg C3 and F7) and inflammation (eg MMP3 and MMP9) in the impaired cortical samples of IS mice. The locomotor promotion in IS zebrafish as well as favorable affinity with key proteins (C3, F7, and MMP9) highlighted anti-IS activities of brain-permeating constituents (senkyunolide I and protocatechuic acid) of GXNT.

Conclusion: Taken together, these intriguing findings indicate that GXNT intervention exerts a beneficial effect against post-IS injury via regulating the complement and coagulation cascades pathway and mobilizing inflammatory network. Senkyunolide I and protocatechuic acid show promise as anti-IS active compounds.

Keywords: Guanxinning tablet, post-ischemic stroke injury, complement and coagulation cascades, inflammatory network mobilization, active substance

Introduction

Globally, ischemic stroke (IS) affected approximately 7.59 million individuals, leading to 3.48 million IS-related deaths, as per data from the Global Burden of Disease Study 2020.[1] Despite enormous effort to manage IS risk factors and optimize IS care, IS assumes the major responsibility for severe long-term disability and high mortality worldwide.[1] Ischemic brain injury involves a series of pathological events, encompassing energy-dependent ion pumps and channels failures, excitotoxicity, calcium overload, mitochondrial dysfunction, increased oxidative stress, destruction of blood–

Received: 10 June 2024
Accepted: 10 September 2024
Published: 18 September 2024

Graphical Abstract

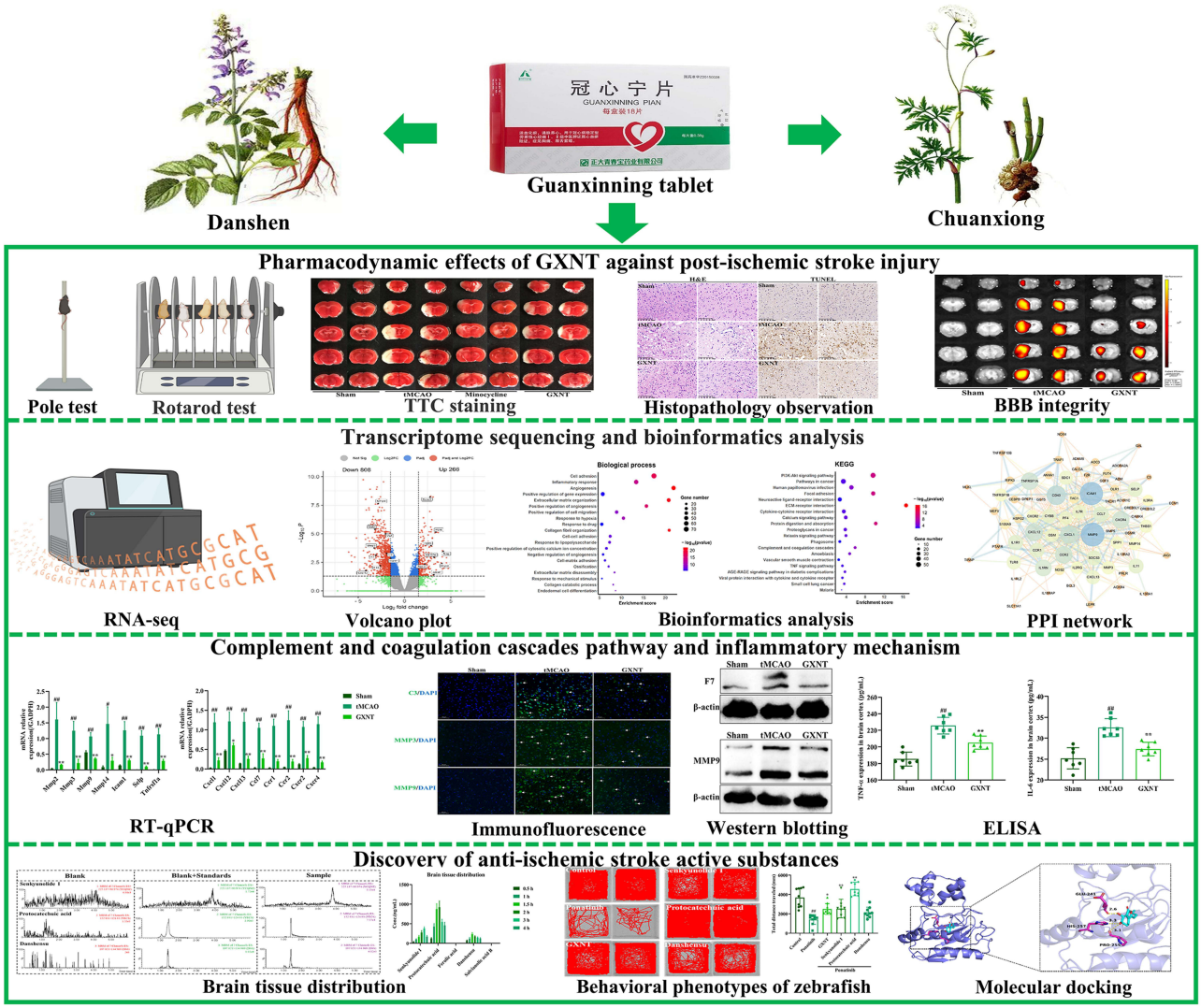

brain barrier (BBB), inflammatory responses, and eventually cell death.[2] Although advances in better understanding the pathogenesis of IS, intravenous thrombolysis and mechanical thrombectomy remain the standard therapeutic options.[3] However, the limitation of thrombolytic therapy (eg narrow therapeutic window, thrombolysis-associated hemorrhagic transformation, and reperfusion injury) urgently calls for alternatives.[4]

In China, *Salvia miltiorrhiza* Bunge (Danshen) and *Ligusticum wallichii* Franch. (Chuanxiong) have been widely employed as representative Chinese medicines to invigorate blood circulation and remove stasis in the context of cardiovascular and cerebrovascular diseases.[5,6] Guanxinning tablet (GXNT), a formulation composed of extracts from Danshen and Chuanxiong in a 1:1 ratio, was approved by the National Medical Products Administration of China in 2015 for treating patients with stable exertional angina pectoris Grade I or II linked to heart-blood stagnation syndrome in traditional Chinese medicine.[7–9] Chemical profiling of GXNT has revealed its major components to be phenolic acids, tanshinones, senkyunolides, terpenes and sugars.[10,11] Pharmacological researches have highlighted GXNT's potential to inhibit atherosclerosis, induce vasodilation, prevent thrombosis, and exert neuroprotective effects.[7,12–14] Recently, Hui et al reported that GXNT pretreatment effectively alleviated acute cerebral ischemia/reperfusion injury (CI/RI) via

inflammatory and oxidative modulation.[15] Li et al found that GXNT treatment obviously improved cognitive behavior, enhanced cerebral vascular status, and protected BBB integrity in an animal model of diabetic encephalopathy.[16] These findings suggested that beyond cardiac protection, GXNT might also contribute to cerebral protection.

Previous studies from our team identified the significant anti-thrombotic and pro-angiogenic activities of GXNT, successfully pinpointing several active compounds (such as senkyunolide I, salvianolic acid B, and ferulic acid) by zebrafish-based phenotypic screening.[11,17] Enlightened by the anti-IS potential of GXNT, we aimed to further assess its pharmacodynamic effects on post-IS functional recovery and brain damage using a mouse model of IS.[18–20] Employing transcriptome sequencing in conjunction with experimental validation, we investigated the possible anti-IS mechanisms of GXNT. Subsequently, we integrated brain tissue distribution analysis of main ingredients (senkyunolide I, protocatechuic acid, ferulic acid, danshensu, and salvianolic acid B), zebrafish-based behavioral verification, and molecular docking to ascertain the bioactive substances responsible for GXNT's anti-IS effect. The present work endeavors to provide potential pharmacological intervention options for enhancing functional recovery following IS.

Materials and Methods

Drugs and Reagents

GXNT (drug approval number: Z20150028; batch number: 2104009) was obtained from Chiatai Qingchunbao Pharmaceutical Co., Ltd. (Hangzhou, China). The detailed preparation method and quality control strictly followed the Standard of National Medical Products Administration of China (YBZ00342016). The representative HPLC chromatogram of GXNT has been reported in our previous study.[11] Minocycline (M102970) was obtained from Aladdin Biochemical Technology Co., Ltd. (Shanghai, China). Senkyunolide I (B21463), ferulic acid (B20007), danshensu (B20254), protocatechuic acid (B21614), and ponatinib (PON, S81149) were bought from Yuanye Biotechnology Co., Ltd. (Shanghai, China). Salvianolic acid B (ABL1692) was purchased from ABPHYTO Biotechnology Co., Ltd. (Chengdu, China). Nitidine chloride (WKQ17120103) was purchased from Weikeqi Biotechnology Co., Ltd. (Chengdu, China). Chloramphenicol (C8050) was purchased from Solarbio Biotechnology Co., Ltd. (Beijing, China). The purities of the above compounds were greater than 98%. Ultra-pure water was pretreated using a Millipore-Q water purification system (Millipore, Milford, MA, USA). Chromatographic-grade methanol (22035147) and acetonitrile (22055247) were obtained from TEDIA. Ethyl acetate (20220311) was bought from GHTECH Co., Ltd. (Shantou, China). Formic acid (P1881926) and hydrochloric acid (P2027782) were bought from Titan Technology Co., Ltd. (Shanghai, China). 2, 2, 2-Tribromoethanol (T48402, purity ≥ 97%) and Evans Blue (E2129, dye content ≥ 75%) were obtained from Sigma (St. Louis, MO, United States). 2, 3, 5-Triphenyl-2H-Tetrazolium Chloride (TTC) solution (2%, G3005) and DAB substrate kit (DA1015) were obtained from Solarbio Biotechnology Co., Ltd. (Beijing, China). Paraformaldehyde fix solution (4%, E672002) was obtained from Sangon Biotechnology (Shanghai, China). In situ cell death detection kit (11684817910) was purchased from Roche. TRIzol reagent (CW0580), HiFiScript cDNA Synthesis Kit (CW2569), and Ultra SYBR Mixture (CW0659) were purchased from CoWin (Beijing, China). Anti-MMP3 (17,873-1-AP), anti-MMP9 (10,375-2-AP), anti-F7 (23,058-1-AP), and anti-C3 (21,337-1-AP) antibodies were purchased from Proteintech Group, Inc. (Wuhan, China). Anti-β-actin antibody (AF2811), HRP-labeled goat anti-mouse IgG H&L (A0216), and HRP-labeled goat anti-rabbit IgG H&L (A0208) were purchased from Beyotime Biotechnology Co., Ltd. (Shanghai, China). 4′,6-diamidino-2-phenylindole (DAPI) solution (HK1032) was purchased from HaoKe Biotechnology Co., Ltd. (Hangzhou, China).

Animals

Adult male C57BL/6J mice (20–22 g) and specific-pathogen-free adult male Sprague Dawley (SD) rats (245–285 g) were purchased from Shanghai SLAC Laboratory Animal Co., Ltd. (Shanghai, China, Certificate No.: SCXK [Hu] 2017–0005). The Laboratory Animal Center of Zhejiang University provided the Wildtype AB strain zebrafish. All animal studies were performed following the guidance of the Care and Use of Laboratory Animals published by the US National Institutes of Health (NIH Publication No.85–23, revised 1996) and the protocols of animal experiments were approved by the Laboratory Animal Welfare and Ethics Committee of Zhejiang University (AP CODE: ZJU20220096).

The mice and rats were housed in an air-conditioned room (25°C ± 1°C, 45% ± 5% relative humidity, 12-hour light/dark cycle) with free access to clean water and food. Embryos were generated through natural spawning, and zebrafish were maintained following standard protocols.[21]

Transient Middle Cerebral Artery Occlusion (tMCAO) Model Establishment and Treatment

The tMCAO model was induced as the previously reported surgical procedure.[20] In short, after exposing the left carotid arteries of the anesthetized mice, a commercial silicone-coated nylon monofilament (diameter with coating 0.18 ± 0.01 mm, L1800, Jialing Biotechnology Co., Ltd., Guangzhou, China) was inserted to obstruct the middle cerebral artery through the external carotid artery, resulting in a decline of local cerebral blood flow to approximately 20% of the baseline. After 60 min of transient focal ischemia, the suture was removed to achieve reperfusion and blood flow returned to approximately 90% of the baseline. The same surgical procedure was carried out in sham-operated mice without inserting the monofilament. Apart from the sham group (n = 25), experimental animals were randomly divided into tMCAO (n = 40), tMCAO + minocycline (n = 15, 45 mg/kg, dissolved in ultrapure water and sterile-filtered through 0.22 μm), and tMCAO + GXNT (n = 35, 700 mg/kg) groups. Through referring to previously reported effective doses against acute CI/RI and diabetic encephalopathy,[15,16] the administration dosage of GXNT was converted according to the clinical dose. Thirty minutes before operation, the mice in GXNT group were orally administered with GXNT in ultrapure water at a dose of 10 mL/kg. 24 h after reperfusion, GXNT-treated mice received 6 consecutive days of dosing at the same dose. For tMCAO + minocycline group, the first intraperitoneal injection was administered 30 min before the operation according to the corresponding dose, and then once daily for 6 days. The sham and tMCAO groups received 0.9% normal saline according to the same administration scheme of GXNT-treated group.

Neurological Function Tests

To estimate the effects of GXNT intervention on neurological deficits of mice after IS modeling, a modified Neurological Severity Score (mNSS) test was executed (n = 10 for each group) as described elsewhere on days 1, 4, and 7, respectively.[18] The neurological deficit score was graded on a scale of 0–18, and a lower score was positively correlated with better neurological outcomes. Based on the score criteria (a score of 9–12 points on post-IS day 1), 7.0% mice were eliminated. Among the selected subjects, 80.4% mice received various tests.

Pole Test

After three consecutive days of training, the pole test was performed using a vertical rough-surfaced wooden pole apparatus (50 cm length, 10 mm in diameter) on post-IS day 6.[22] Briefly, ten mice from each group were placed orderly at the top of the climbing pole and the time to descend to the horizontal support was recorded. Three repeated trials were performed for each mouse and the average time was calculated. A maximum time of 30s was allocated to mice that dropped or slipped from the apparatus.

Rotarod Test

The rotarod test was executed to observe the coordinated movements of mice at 5th day after cerebral ischemia.[23] In brief, the mice from each group (n = 10) were placed on the accelerating rotarod with the rotational speed set as slowly increasing from 4 rpm to 40 rpm in 300 s. The average time latency to fall in three repeated trials was recorded for statistical analysis.

TTC Staining

After completing the final mNSS test, the brains from six mice in each group were rapidly acquired to cut into five 2 mm-thickness coronal slices using a rodent brain matrix. Then, TTC staining of sections was performed with 2% TTC solution for 10 min in a 37 °C incubator. The images of stained slices were captured and ImageJ software was used to calculate the infarct volume. Cerebral infarction (%) = total infarction volume /total cerebral volume × 100%.[24]

BBB Integrity Evaluation

The Evans Blue (EB) leakage method combined with fluorescent imaging detection were adopted to evaluate the BBB integrity.[25,26] After performing mNSS test on day 4, seven mice of each group received intravenous injection with 1% EB solution at a dose of 20 mL/kg. Twenty-four hours later, the brains were perfused and sliced into five 2 mm-thick coronal sections. The IVIS® Spectrum In Vivo Imaging System (PerkinElmer, United States) was applied to scan the EB-stained sections followed by the measurement of fluorescence intensity of EB leakage using the Living Image® Software (Version 4.3.1).

Histopathology Observation

At 7th day after tMCAO, the brain samples (n = 4 for each group) were obtained. After tissue fixation, dehydration, paraffin embedding, section, and hematoxylin and eosin (H&E) staining, the histopathology images were captured using an automatic digital slide scanning system (KF-PRO-120, KFBIO, China).

Apoptosis Assay

Terminal deoxynucleotidyl transferase dUTP nick end labeling (TUNEL) detection was performed according to the standard procedure.[27] In brief, the sections were treated with proteinase K for 30 min at 37°C after dewaxing and rehydration. Following incubation with TUNEL reaction mixture for 60 min in a 37°C incubator, the slices were treated in turn with converter-POD solution and diaminobenzidine substrate. The automatic digital slide scanning system (KF-PRO-120, KFBIO, China) was used to randomly acquire the images from five selected fields of damaged cortical areas. The apoptotic index (%) = (TUNEL-positive apoptotic cell number/total cell number) ×100%.

Transcriptome Sequencing

At 7th day after cerebral ischemia, the damaged cortical samples in tMCAO and tMCAO + GXNT groups (n = 3 for each group) were immediately harvested for total RNA extraction and RNA quality was estimated to construct the transcriptomics sequencing library. After quality assurance, the library was sequenced using an Illumina Novaseq platform. Removing the adapter sequence, reads containing ploy-N, and the low-quality reads from raw data to obtain the clean reads. Reads mapping to the reference genome was completed using HISAT2 software (http://daehwankimlab.github.io/hisat2/). FeatureCounts (http://subread.sourceforge.net/) was used to count the number of reads mapped to each gene. Differential expression analysis between the two groups was carried out using the DESeq2 software (http://bioconductor.org/packages/release/bioc/html/DESeq2.html). In this work, $|\log_2\text{FoldChange}| \geq 1.5$ and $Padj < 0.05$ were set as the threshold for the definition of differentially expressed genes (DEGs).

Bioinformatics Analysis

A volcano plot was generated using an online platform for data analysis and visualization (https://www.bioinformatics.com.cn) to display the DEGs. The online platform of NovoMagic (https://magic.novogene.com) was used for hierarchical clustering analysis. The acquired relative expression data of DEGs were visualized as a tree heat map. To further uncover the significant biological processes and functional pathways linked to the efficacy of GXNT on post-IS functional recovery, the online Database for Annotation, Visualization and Integration Discovery (DAVID) bioinformatics tool (Version 6.8, http://david.ncifcrf.gov/) was employed for the Gene Ontology (GO) and Kyoto Encyclopedia of Genes and Genomes (KEGG) enrichment analyses.[28] The protein–protein interaction (PPI) network data were acquired using the Search Tool for Recurring Instances of Neighboring Genes (STRING) database (http://string-db.org/). The PPI network and key nodes of the network ranked by the topological analysis methods of maximal clique centrality (MCC) and Degree were plotted using Cytoscape software (Version 3.7.2).[29]

Real-Time Quantitative Polymerase Chain Reaction (RT-qPCR) Analysis

The total RNA was isolated from the cortical samples using the TRIzol method followed by reverse transcription. Next step, RT-qPCR was performed with the Ultra SYBR Mixture using Bio-Rad CFX Maestro 1.1 Software (Version

Table 1 Primer Sequences for RT-qPCR

Primer name	Forward primer (5′–3′)	Reverse primer (5′–3′)
Vwf	CTTCTGTACGCCTCAGCTATG	GCCGTTGTAATTCCCACACAAG
Thbd	CTCTCCGCACTAGCCAAGC	GGAGCGCACTGTCATCAAATG
Serpine1	TTCAGCCCTTGCTTGCCTC	ACACTTTTACTCCGAAGTCGGT
F10	AGGACTCGGAGGGCAAACT	TCACGGACCTCTTCATAAGAACA
A2m	AAAGGAAATCGCATCG	CATGTTCATTGTCACGGTTT
F7	AAAGGCGTGCCAACTCACTC	CCTACGTTCTGACATGGATTCG
C3	CCAGCTCCCCATTAGCTCTG	GCACTTGCCTCTTTAGGAAGTC
Procr	GTAAGTTTCCGGCCAAAGACT	TCCCCTCAGACCTTTCATGTTT
Serping1	TAGAGCCTTCTCAGATCCCGA	ACTCGTTGGCTACTTTACCCA
Tfpi	CAGGCGTCGGGATTATCGTG	TTCCCCCACATCCAGTGTAGT
Mmp2	CAAGTTCCCCGGCGATGTC	TTCTGGTCAAGGTCACCTGTC
Mmp3	ACATGGAGACTTTGTCCCTTTTG	TTGGCTGAGTGGTAGAGTCCC
Mmp9	CACGGCAACGGAGAAGGCAAAC	CCTGGTCATAGTTGGCTGTGGTGGC
Mmp14	CAGTATGGCTACCTACCTCCAG	GCCTTGCCTGTCACTTGTAAA
Icam1	GTGATGCTCAGGTATCCATCCA	CACAGTTCTCAAAGCACAGCG
Selp	CATCTGGTTCAGTGCTTTGATCT	ACCCGTGAGTTATTCCATGAGT
Tnfrsf1a	CCGGGAGAAGAGGGATAGCTT	TCGGACAGTCACTCACCAAGT
Cxcl1	CTGGGATTCACCTCAAGAACATC	CAGGGTCAAGGCAAGCCTC
Cxcl12	TGCATCAGTGACGGTAAACCA	TTCTTCAGCCGTGCAACAATC
Cxcl13	GGCCACGGTATTCTGGAAGC	GGGCGTAACTTGAATCCGATCTA
Ccl7	GCTGCTTTCAGCATCCAAGTG	CCAGGGACACCGACTACTG
Ccr1	CTCATGCAGCATAGGAGGCTT	ACATGGCATCACCAAAAATCCA
Ccr2	GGTCATGATCCCTATGTGG	CTGGGCACCTGATTTAAAGG
Cxcr2	ATGCCCTCTATTCTGCCAGAT	GTGCTCCGGTTGTATAAGATGAC
Cxcr4	GAAGTGGGGTCTGGAGACTAT	TTGCCGACTATGCCAGTCAAG
GAPDH	TGGTGAAGCAGGCATCTGAG	TGCTGTTGAAGTCGCAGGAG

4.1.2433.1219). The gene glyceraldehyde 3-phosphate dehydrogenase (GAPDH) was employed as normalization and the relative mRNA expression levels of DEGs were analyzed using the $2^{-\Delta\Delta CT}$ method. The details of primer sequences were described as follow in Table 1.

Immunofluorescence Staining

After a series of standard procedures, the tissue slices were incubated overnight at 4°C with anti-C3 (1:200), anti-MMP3 (1:100), and anti-MMP9 (1:200) antibodies. Following treatment with the secondary antibody, cell nuclei were counter-stained with DAPI solution at room temperature for 10 min in dark. Images were acquired and observed using a Pannoramic SCAN II automatic digital slide scanning system (3DHISTECH Ltd., Budapest, Hungary). The mean fluorescence intensity in five random regions was calculated with ImageJ software.[20]

Western Blotting

The total protein extraction and measurement of the damaged cortical tissues were performed according to standard procedures.[20] After protein separation, transmembrane, and blocking, the polyvinylidene fluoride membranes (Millipore, Billerica, MA, USA) were treated overnight at 4°C with anti-MMP9 (1:1000), anti-F7 (1:500), and anti-β-actin (1:1000) antibodies. Following incubation with the corresponding secondary antibody, the enhanced chemiluminescence method was applied to detect and visualize the target protein expression. The quantification of band intensity was performed using Image Lab image processing software (Version 6.0, Bio-Rad Laboratories Inc., USA).

Enzyme-Linked Immunosorbent Assay (ELISA)

The peri-infarcted cortical samples from different groups were weighed, homogenized, and centrifuged to collect the supernatants. Then, mouse IL-6 (ZC-37988, ZCi Biotechnology Co., Ltd.) and TNF-α (ZC-39024, Biotechnology Co., Ltd). ELISA kits were employed to measure the protein concentrations of IL-6 and TNF-α in samples according to the manufacturer's instructions.

Establishment of Zebrafish Model of is and Assessment of Motor Behavior

Ponatinib-induced zebrafish model of IS was established as previously reported.[21,30] In brief, 12–15 zebrafish embryos of 6 days post fertilization (dpf) of per well were collected into a 12-well plate and treated with 1 μg/mL ponatinib for 24 h to induce cerebral ischemia. Based on the toxicity test, GXNT (500 μg/mL) and its active substances (senkyunolide I 50 μg/mL, protocatechuic acid 100 μg/mL, danshensu 200 μg/mL) were supplemented for co-incubation. Dimethyl sulfoxide (DMSO, 0.1% v/v final concentration) was added in the control group. 24 h later, the locomotor behavior test of zebrafish was performed using a DanioVision system with EthoVision XT software (Noldus Information Technology Co., Ltd., Wageningen, Netherlands). Free-swimming activity of zebrafish was automatically recorded within a data collection time of 30 min.

Molecular Docking

The ChemOffice software (Version 19.0) was used to generate three-dimensional structures of active substances (senkyunolide I and protocatechuic acid) in mol2 format. The X-ray crystal structures of target proteins (F7, C3, and MMP9) were retrieved from the Protein Data Bank (PDB) database (http://www.rcsb.org/pdb/) and the PDB format files were downloaded. After dehydration, hydrogenation and other operations using the AutoDock (4.2.6) software, the files of protein receptors and ligands were saved in PDBQT format. The AutoDock Vina (1.2.0) software was used for docking and analysis of the binding activities of receptors and ligands. The PyMOL 2.5 software was used to exhibit the docking results.

Brain Tissue Distribution Analysis

Instruments and Analytical Conditions

Biological samples were detected using an ACQUITY UPLC® H Class system, which was coupled to a Xevo TQ-S micro triple quadrupole mass spectrometer (Waters, Milford, MA, USA) equipped with an electrospray ionization (ESI) source and a MassLynxTM workstation software (Version 4.2, Waters, Milford, MA, USA).

The chromatographic separation was carried out using a Waters Acquity UPLC HSS T3 column (2.1 × 50 mm, 1.7 μm), and the column temperature was maintained at 35°C. The mobile phase consisted of 0.1% formic acid aqueous solution (A) and acetonitrile (B). The gradient elution program was set as follows: 0.00–2.00 min, 20%–60% B; 2.00–3.50 min, 60%−80% B; 3.50–4.50 min, 80% B; 4.50–4.51 min, 80%–20% B; 4.51–6.00 min, 20% B. The flow rate was kept at 0.2 mL/min, and the injection volume was 2 μL.

Mass spectrometric detection was performed in multiple reaction monitoring (MRM) mode. The MRM transitions and parameters for the detection of five analytes and internal standards were listed in Table 2. Senkyunolide I and nitidine

Table 2 MRM Transitions and Parameters for the Detection of 5 Analytes and Internal Standards

Analytes	Precursor ion (m/z)	Product ion (m/z)	Cone voltage (V)	Collision energy (eV)
Senkyunolide I	225.14	90.97	32	32
Protocatechuic acid	152.93	124.93	42	10
Ferulic acid	192.96	133.97	44	12
Danshensu	197.02	134.97	48	20
Salvianolic acid B	717.25	519.21	10	18
Nitidine chloride (internal standard)	406.38	300.38	14	26
Chloramphenicol (internal standard)	321.04	151.95	68	16

chloride (internal standard) were monitored in positive mode, whereas protocatechuic acid, ferulic acid, danshensu, salvianolic acid B, and chloramphenicol (internal standard) were monitored in negative mode.

Preparation of Standard Solutions, Calibration Standards and Quality Control Samples

The stock solutions (0.2 mg/mL) of senkyunolide I, protocatechuic acid, ferulic acid, danshensu, and salvianolic acid B were separately prepared in methanol and then serially diluted with methanol to obtain working solutions (10000, 5000, 2500, 1250, 625, 312, and 156 ng/mL) used for method validation. The stock solutions (0.2 mg/mL) of internal standards and working solutions (100 ng/mL for nitidine chloride and 1000 ng/mL for chloramphenicol) were prepared as described in the above mentioned method. Calibration samples were prepared by adding different concentrations of working solutions into blank tissue homogenates. Quality control samples at different concentrations were prepared according to the preparation method of calibration samples.

Sample Preparation

The tissue samples were weighed to 0.1 g and homogenized with pre-cooled saline solution (1:9, w/v) using a tissue homogenizer. After centrifuging at 13400 rpm for 10 min, the tissue homogenates (200 μL) were transferred to 1.5 mL EP tubes followed by adding 10 μL of the solutions of internal standards containing 1 μg/mL chloramphenicol and 100 ng/mL nitidine chloride. After uniformly mixing, the mixture was acidized with 10 μL of 1M hydrochloric acid and then extracted with 1 mL of ethyl acetate. After vortex mixing for 3 min, the mixture was centrifuged at 13400 rpm for 10 min, and 1 mL of the upper organic layer was transferred to the new EP tubes and dried with nitrogen at 35°C. The residue was re-dissolved in 200 uL MeOH-H2O (50:50, v/v) followed by vortex mixing for 1 min and centrifuging at 13400 rpm for 10 min. Finally, the supernatant was taken and transferred to a 200 μL liquid glass lined tube for UPLC-MS/MS analysis.

Method Validation

The method applied in biological samples was validated based on the guidelines of US Food and Drug Administration bioanalytical method validation, including specificity, linearity and lower limit of quantification, accuracy and precision, matrix effect and extraction recovery, and stability.[31]

Brain Tissue Distribution Study

After fasting for 12 h, forty-two SD rats were randomly divided into seven groups (n = 6 per group). Following a single intragastric administration of GXNT (9.576 g/kg), the brain tissues were harvested at 0 h, 0.5 h, 1 h, 1.5 h, 2 h, 3 h, and 4 h. The tissues were rinsed with pre-cooled saline solution and blotted with filter paper. The tissues were stored at −80°C until analysis.

Statistical Analysis

SPSS software (Version 16.0, SPSS, Inc., Chicago, IL, United States) was employed for the statistical analysis. The comparison between two groups was performed with the Student's two-tailed *t*-test. The one-way analysis of variance (ANOVA) followed by Dunnett's *t*-test was used for comparisons among multiple groups. A value of $P < 0.05$ was defined as statistically significant. The concentrations of main components in brain tissues were calculated using the calibration curve method. All the graphs were generated using GraphPad Prism 7 software (GraphPad Software, Inc., La Jolla, CA, United States).

Results

GXNT Treatment Alleviated the Neurological Deficits and Locomotor Dysfunction in Post-IS Mice

The neurobehavioral tests were performed to assess the brain functional outcomes in each group (Figure 1A). In contrast to the normal behaviors observed in sham-operated mice, cerebral ischemia and reperfusion seriously damaged neurological and motor functions. Throughout the entire experimental period, mice subjected to tMCAO were unable to successfully complete the tests and exhibited the highest scores (Figure 1B). Similar to the efficacy of minocycline, continuous intervention with GXNT (700 mg/kg) noticeably improved brain functional outcomes in tMCAO mice on post-IS days 4 and 7 compared to the model

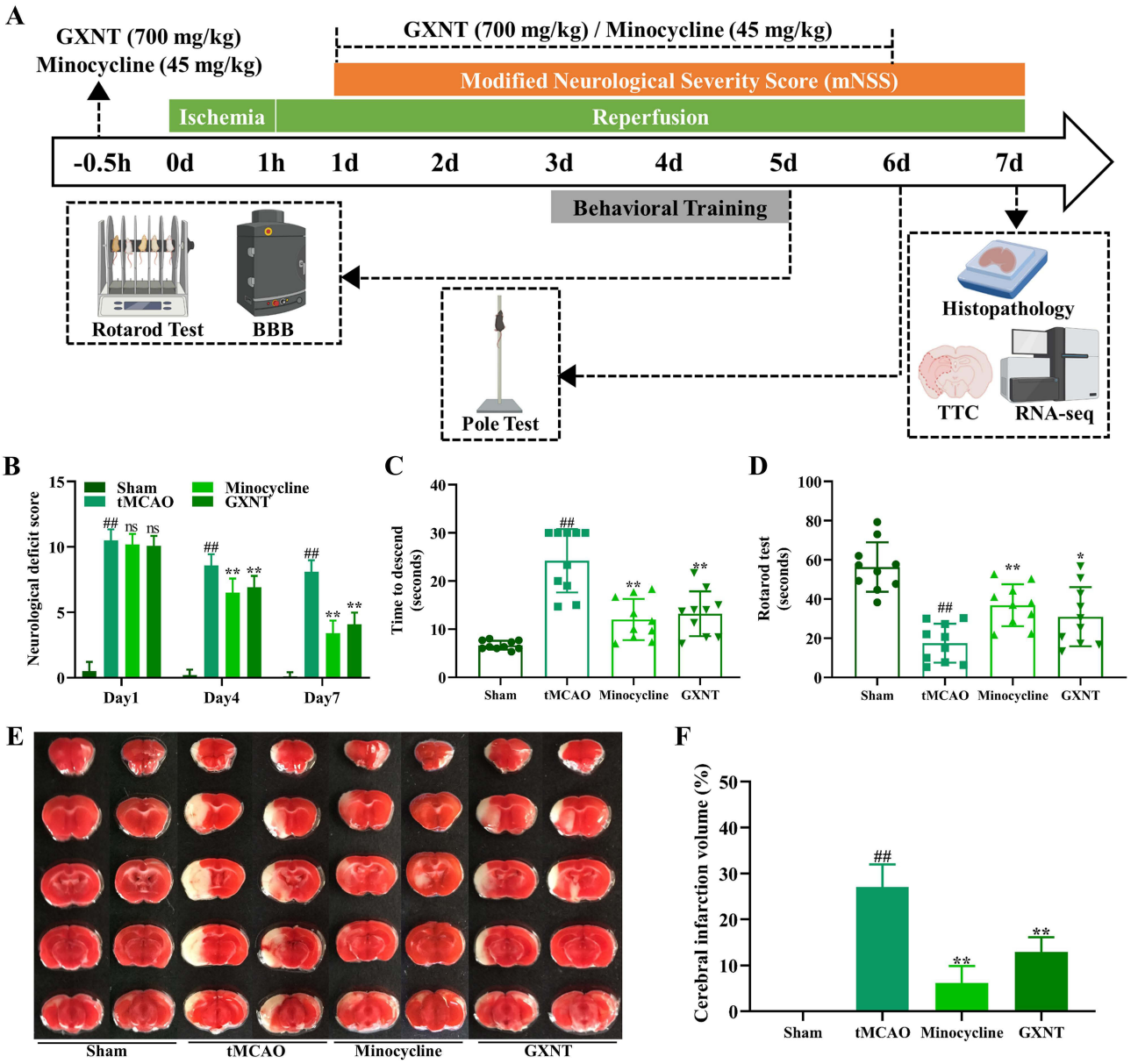

Figure 1 Treatment with GXNT facilitated the functional recovery and lowered the infarct volumes in post-IS mice. (**A**) The schematic diagram of experimental design. (**B**) The neurological outcomes were assessed by mNSS test (n = 10). Compared with the model group, experimental IS mice receiving GXNT treatment behaved a better neurological function on post-IS days 4 and 7. Bar graph representing results of pole test (**C**) and rotarod test (**D**) (n = 10). Compared with the model group, a significant improvement of motor function was observed in GXNT-treated mice. (**E**) The typical images of TTC staining of each group (n = 6). The white color represented the infarction zone. (**F**) The quantitative analysis of TTC staining (n = 6). As expected, GXNT treatment obviously reduced the infarction volumes induced by tMCAO operation. Data are presented as the mean ± SD. $^{\#\#}P < 0.01$ versus the sham group; $^{*}P < 0.05$, and $^{**}P < 0.01$ versus the tMCAO group.

group (Figure 1B). In addition, pole and rotarod experiments demonstrated that tMCAO mice exhibited a clear deficit in locomotor coordination (Figure 1C and D). In comparison to sham-operated mice, tMCAO-treated mice took longer to climb to the bottom of the pole and spent less time staying on the accelerating rotarod (Figure 1C and D). As anticipated, both minocycline and GXNT significantly enhanced the motor coordination of tMCAO mice (Figure 1C and D). These data suggested that continuous GXNT treatment contributed to the improvement of neurological and motor functions in mice with IS.

GXNT Treatment Reduced Brain Lesions in Post-IS Mice

To assess the effects of GXNT against brain lesions caused by tMCAO operations, TTC staining and histopathology analysis were performed. The representative TTC-stained images (Figure 1E) and the corresponding quantization

outcomes (Figure 1F) revealed an obvious increase in infarction regions, with a white color following cerebral ischemia and reperfusion, compared to those in the sham group. Conversely, the notably reduced infarction volumes were observed in tMCAO mice receiving minocycline and GXNT treatment (Figure 1E and F). Subsequent pathological examination indicated evident damages to tissue and neuron morphology due to experimental IS. This included the generation of numerous vacuolated spaces, a disordered and sparse arrangement of cells, and neurons with karyopyknosis (Figure 2A). Encouragingly, GXNT treatment partially reversed these aforementioned pathological changes (Figure 2A). In addition to H&E staining, TUNEL staining was employed to identify apoptotic neurons. As illustrated in Figure 2A and D, the number of TUNEL-positive neurons (brown-yellow color) observably elevated in the damaged cortex of tMCAO mice, compared to the sham group. However, GXNT intervention obviously decreased the presence of TUNEL-stained neurons. These results suggested that the administration of GXNT effectively attenuated brain damages induced by IS.

GXNT Treatment Protected BBB Integrity in Post-IS Mice

As a crucial pathophysiological hallmark of IS, BBB breakdown contributes to the development of brain injury and subsequent functional outcomes.[32] To evaluate BBB permeability, we utilized the previously established approach of EB extravasation combined with a rapid fluorescence imaging detection.[25] In contrast to the intact BBB observed in the sham group, significant disruption of BBB was present in the model group, characterized by EB leakage and detectable spectrum (Figure 2B and C,E). As expected, successive administration of GXNT at a dosage of 700 mg/kg significantly reduced damage to BBB integrity when compared to the model group (Figure 2B and C,E). These findings indicated that GXNT treatment contributed to a reduction in BBB permeability.

Transcriptomic Study Revealed Functional Mechanisms of GXNT Against Post-IS Injury

To gain deeper insights into the underlying molecular mechanisms responsible for the favorable impacts of GXNT in mitigating post-IS injury, we conducted transcriptome sequencing on cortical samples from both the tMCAO and GXNT treatment groups. The volcano plot revealed a total of 1074 DEGs, meeting the criteria of $|\log2FoldChange| \geq 1.5$ and $Padj < 0.05$, with 808 down-regulated genes and 266 up-regulated genes in the GXNT group as compared to the tMCAO group (Figure 3A). A tree heat map was presented for the visualization of representative DEGs information (Figure 3B). Subsequently, the list of DEGs was subjected to comprehensive bioinformatics analysis using DAVID. The top-ranking GO terms highlighted significant biological processes, such as angiogenesis, extracellular matrix organization, cell adhesion, and inflammatory response. These biological processes exhibited enriched DEGs and elevated enrichment scores, underscoring their relevance to the anti-IS action of GXNT (Figure 3C). The results of the KEGG pathway enrichment analysis unveiled pivotal signaling pathways potentially regulated by GXNT in response to post-IS injury, including ECM–receptor interaction, focal adhesion, PI3K-Akt signaling, and complement and coagulation cascades. Furthermore, cytokine–cytokine receptor interaction and TNF signaling pathway emerged as closely associated with inflammation (Figure 3D). Combined, these biological processes and functional pathways were strongly connected to the therapeutic efficacy of GXNT, warranting comprehensive analysis through in-depth experimental validation.

GXNT Regulated the Complement and Coagulation Cascades Pathway

Accumulating evidence underscored the close association between the complement and coagulation cascades and IS as well as post-IS injury.[33,34] Intriguingly, KEGG analysis suggested that the complement and coagulation cascades exhibited relatively higher enrichment scores, and potentially represented a pivotal molecular mechanism regulated by GXNT treatment (Figure 3D). Subsequently, a PPI network was constructed for the 18 DEGs enriched in complement and coagulation cascades (Figure 4A). As illustrated in Figure 4B and Supplementary Figure S1, the top 10 nodes within the network determined through a Degree-based topological analysis, included Vwf, Thbd, Serpine1, F10, A2m, F7, C3, Procr, Serping1, and Tfpi. Next, to validate the regulatory impact of GXNT on these identified DEGs, a series of techniques including RT-qPCR, western blotting, and immunofluorescence staining were employed. Comparative analysis revealed elevated transcriptional levels of genes associated with the complement and coagulation cascades in the damaged cortical samples, as compared to the sham group (Figure 4C). Remarkably, intervention with GXNT (700 mg/kg) effectively attenuated the abnormally elevated mRNA levels of these genes in IS mice, which was consistent with the results of RNA-seq results (Figure 4C). In addition, the

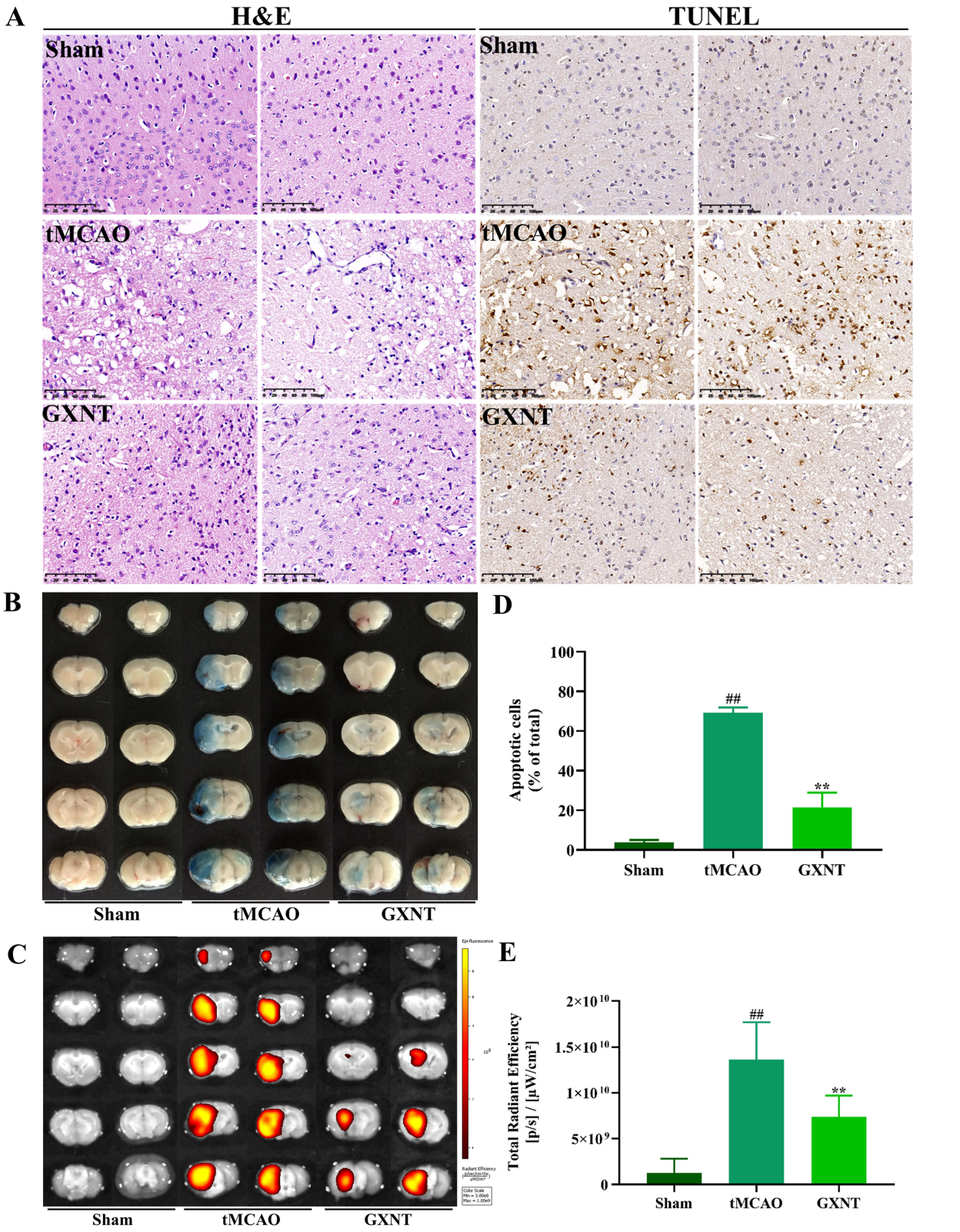

Figure 2 GXNT treatment mitigated pathological changes and BBB breakdown caused by IS. (**A**) The representative images of H&E staining and TUNEL staining (×200 magnification, scale bar: 100 μm, n = 4). Compared with the model group, GXNT intervention effectively reduced the pathological injury and neuronal apoptosis of cortex in IS mice. (**B**) The representative images of EB-stained slices (n = 7). (**C**) The corresponding fluorescent images of EB extravasation (n = 7). (**D**) Quantification of TUNEL-positive apoptotic cells in damaged cortex (n = 4). (**E**) Quantification of fluorescent images of EB extravasation (n = 7). Compared with the model group, GXNT administration observably lowered the BBB disruption in IS mice. Data are presented as the mean ± SD. $^{\#\#}P < 0.01$ versus the sham group; $^{**}P < 0.01$ versus the tMCAO group.

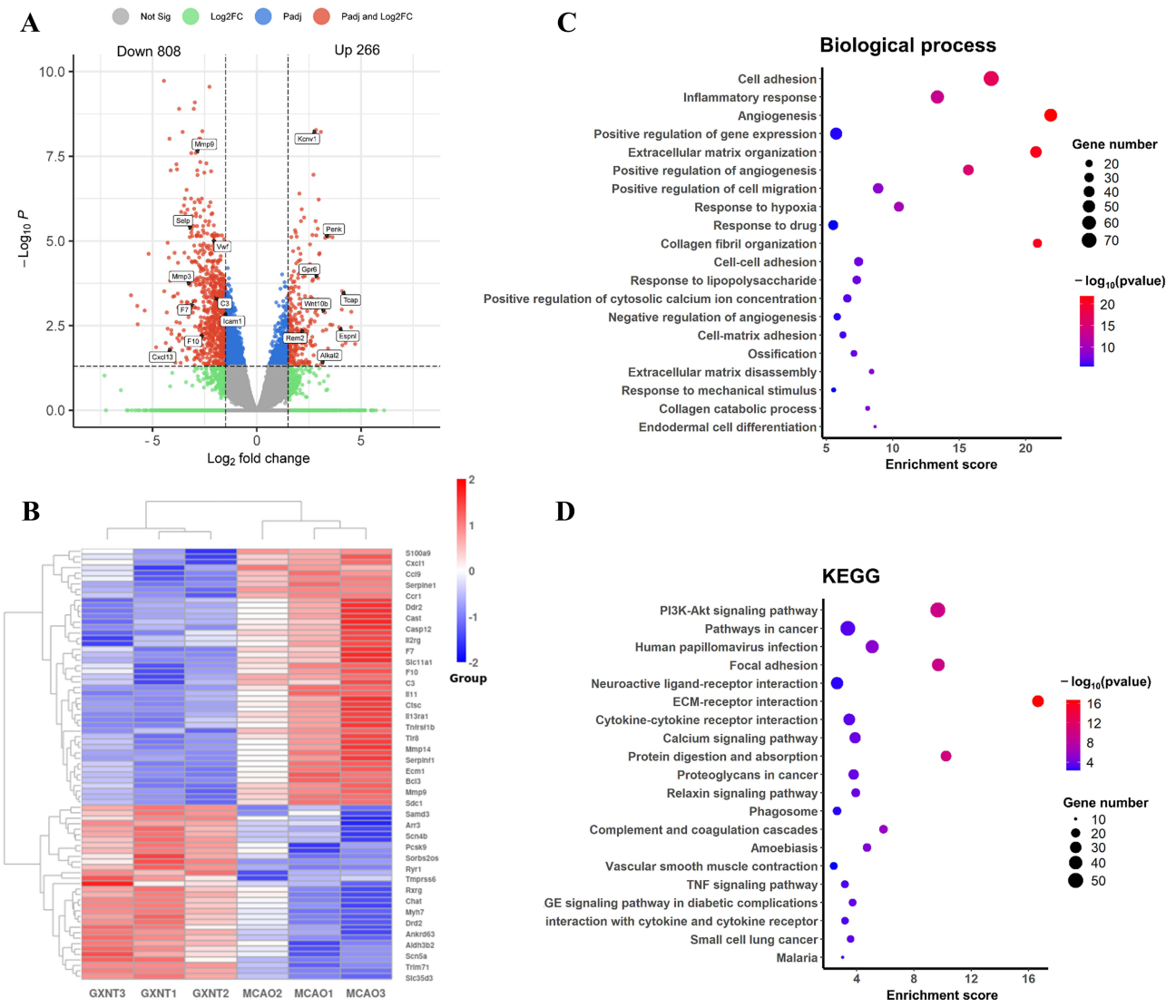

Figure 3 RNA-seq identification of DEGs and bioinformatics analysis. (**A**) Volcano plot of DEGs in GXNT group compared to tMCAO group. According to the screening criteria of |log2FoldChange| ≥ 1.5 and *Padj* < 0.05, 808 down-regulated DEGs and 266 up-regulated DEGs were identified. (**B**) A tree heat map of hierarchical clustering analysis of partial DEGs between GXNT group and tMCAO group. Red color represented up-regulated DEGs and blue color represented down-regulated DEGs. (**C**) GO enrichment analysis of 1074 DEGs. Top 20 significantly enriched biological processes were ranked based on the enrichment score and enriched gene numbers. (**D**) KEGG pathway enrichment analysis of 1074 DEGs. Top 20 significantly enriched signaling pathways were ranked based on the enrichment score and enriched gene numbers. Among them, complement and coagulation cascades, TNF signaling pathway were the important pathways underlying the beneficial effects of GXNT against post-IS injury.

increased protein expression levels of coagulation factor VII (F7) and complement component 3 (C3) were detected in the damaged cortex of IS mice, as compared to those in sham-operated mice (Figure 4D-G). However, treatment with GXNT at a dose of 700 mg/kg notably reduced the dysregulated expression levels of key proteins, namely F7 and C3 (Figure 4D-G). Collectively, these data indicated that the anti-IS effect of GXNT might be partially linked to its regulatory influence on the complement and coagulation cascades signaling pathway.

GXNT Treatment Inhibited Post-IS Inflammation

The significance of inflammation across various stages of IS has been proved by a series of preclinical and clinical evidence.[35] Based on the results of bioinformatics analysis of DEGs, pathways associated with inflammatory response (such as cytokine–cytokine receptor interaction and the TNF signaling pathway) were highly enriched, highlighting the potential of GXNT in targeting post-IS inflammation (Figure 3C and D). Hence, we established a PPI network encompassing 86 DEGs related to inflammation (Figure 5A). Through the amalgamation of topological analysis methods, including Degree and MCC, coupled

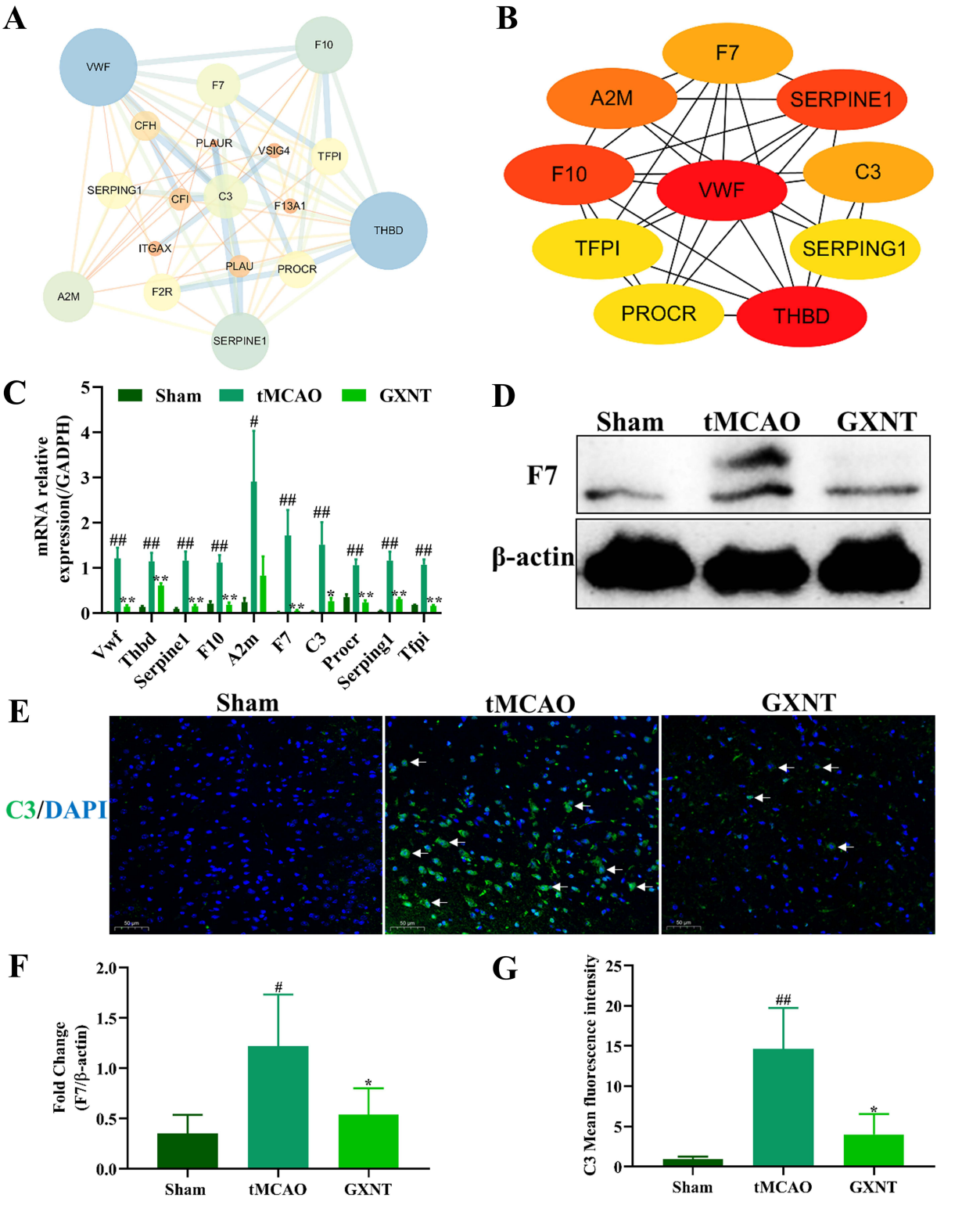

Figure 4 Treatment with GXNT attenuated post-IS injury partly via the regulation of complement and coagulation cascades pathway. (**A**) The PPI network construction of 18 DEGs enriched in complement and coagulation cascades. (**B**) Determination of top 10 nodes based on topological analysis method of Degree. The node with deeper color represented the more importance in the network. (**C**) The relative mRNA expression levels of key DEGs related to complement and coagulation cascades were verified using RT-qPCR (n = 5). (**D**) The representative images of Western blotting of F7 (n = 4). (**E**) The representative images of immunofluorescent staining of C3 protein expression in cerebral sections (×630 magnification, scale bar: 50 μm, n = 3). The white arrows represented immune-positive cells. (**F**) Quantification of Western blotting of F7 protein expression in cortical samples (n = 4). (**G**) Quantification of immunofluorescent staining of C3 protein expression (n = 3). Intervention with GXNT effectively regulated the abnormal mRNA and protein levels of complement and coagulation cascades related DEGs compared to those in the tMCAO group. RT-qPCR results are expressed as mean ± SEM. Data of Western blotting and immunofluorescence are presented as the mean ± SD. $^{\#}P < 0.05$, and $^{\#\#}P < 0.01$ versus the sham group; $^{*}P < 0.05$, and $^{**}P < 0.01$ versus the tMCAO group.

https://doi.org/10.2147/DDDT.S479881 DovePress

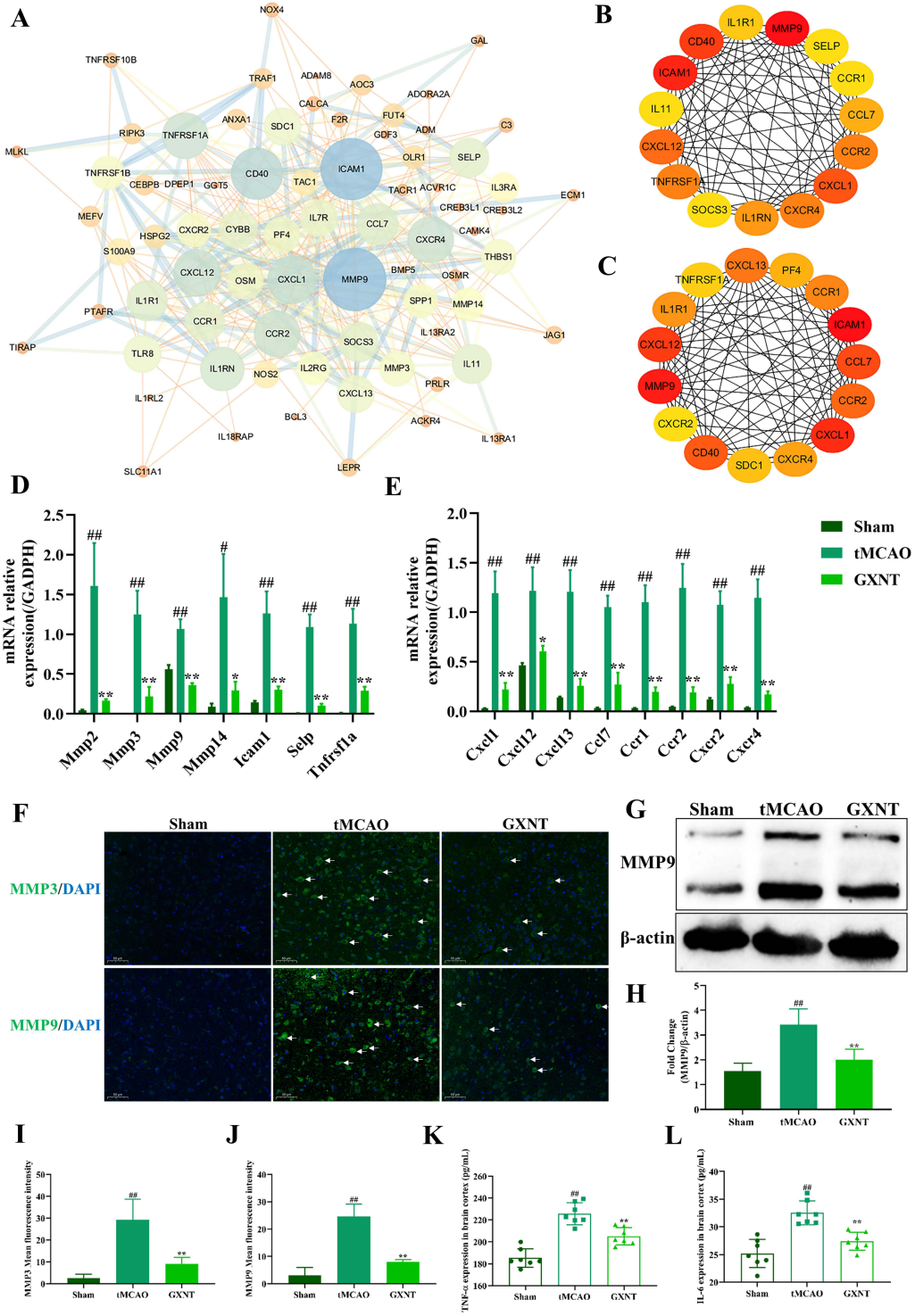

Figure 5 Intervention with GXNT reduced post-IS inflammation. (**A**) The PPI network construction of 86 inflammation related DEGs. (**B**) Determination of top 15 nodes based on topological analysis method of Degree. The more important node in the network presented the deeper color. (**C**) Determination of top 15 nodes based on topological analysis method of MCC. The deeper color was positive correlation with the importance in the network. (**D-E**) RT-qPCR results of inflammation related key DEGs (n = 5). (**F**) The representative images of immunofluorescent staining of MMP3 and MMP9 protein expression levels in cerebral sections (×630 magnification, scale bar: 50 μm, n = 3). The white arrows represented immune-positive cells. (**G**) The representative images of Western blotting of MMP9 (n = 4). (**H**) Quantification of Western blotting of MMP9 protein expression in cortical samples (n = 4). Quantification of immunofluorescent staining of MMP3 (**I**) and MMP9 (**J**) protein expression levels (n = 3). Compared with the model group, GXNT treatment obviously inhibited the abnormal changes of mRNA and protein levels of inflammation related DEGs. The detection of TNF-α (**K**) and IL-6 (**L**) contents in impaired cortical tissues (n = 7). RT-qPCR results are expressed as mean ± SEM. Data of Western blotting, immunofluorescence, and ELISA are presented as the mean ± SD. $^{\#}P < 0.05$, and $^{\#\#}P < 0.01$ versus the sham group; $^{*}P < 0.05$, and $^{**}P < 0.01$ versus the tMCAO group.

with insights from the literature review supplementation, major targets associated with inflammation, including matrix metalloproteases (Mmp2, Mmp3, Mmp9, Mmp14), adhesion molecules (Icam1, Selp), chemokines (Cxcl1, Cxcl12, Cxcl13, Ccl7, Ccr1, Ccr2, Cxcr2, Cxcr4), and Tnfrsf1a, were identified as potential targets regulated by GXNT (Figure 5B and C and Supplementary Figure S2). Consistent with the sequencing findings, the transcriptional levels of proinflammatory mediators were markedly diminished following GXNT treatment compared to those in tMCAO group (Figure 5D and E). Immunofluorescence staining and Western blotting experiments demonstrated that GXNT intervention significantly reversed the abnormal elevation of matrix metallopeptidase 3 (MMP3) and matrix metallopeptidase 9 (MMP9) proteins in damaged cortical samples induced by ischemia and reperfusion (Figure 5F-J). In addition, GXNT treatment also significantly reduced the increase of tumor necrosis factor-α (TNF-α) and interleukin-6 (IL-6) contents in impaired cortices of tMCAO mice (Figure 5K and L). In sum, these data indicated that GXNT exerted anti-inflammatory roles which might contribute to its efficacy against IS.

Identification of Active Substances in GXNT Against Post-IS Injury

In light of observed beneficial effects of GXNT in ameliorating post-IS injury, an integrated approach involving brain tissue distribution analysis of main ingredients (senkyunolide I, protocatechuic acid, ferulic acid, danshensu, and salvianolic acid B), zebrafish behavioral validation, and molecular docking was employed to further determine the active substances in GXNT contributing to its anti-IS efficacy. As displayed in Figure 6A and B, senkyunolide I, protocatechuic acid, and danshensu were rapidly detected in the brain tissues after oral administration of GXNT using the established analytical method (Supplementary Table S1-S4). However, ferulic acid and salvianolic acid B were not discernible in the brain samples during the detection time. Subsequently, the behavioral improvement potential of these constituents was evaluated in a zebrafish model of IS. The results showed that treatment with either senkyunolide I or protocatechuic acid notably ameliorated the behavioral abnormalities of zebrafish model of IS. This was manifested by enhanced total swimming distance, average speed of motion, and movement time (Figure 6C-F). In addition, molecular docking results showed that the binding energies of ligands (senkyunolide I, protocatechuic acid) and receptor proteins (C3, F7, MMP9) were all less than −5 kcal/mol, indicating good affinity between these components (senkyunolide I, protocatechuic acid) and key target proteins (C3, F7, MMP9) (Figure 6G-L). Therefore, senkyunolide I and protocatechuic acid emerged as major active substances of GXNT against post-IS injury.

Discussion

Despite the advancements in contemporary rehabilitation strategies, IS continues to be the primary driver of functional deterioration, limited mobility, psycho-social complications, and reduced quality of life.[36] Currently, consensus remains elusive regarding the optimal neuro-rehabilitation interventions for improving post-IS outcomes.[36] Neuroprotective strategies entail interventions aimed at preventing acute brain ischemic injury, neuronal loss, and fostering neuro-regeneration and functional recovery by intervening in detrimental molecular events arising from ischemia and reperfusion.[2,37] Although numerous preclinical studies underscore the promising potential of several neuroprotectants, successful translation from the laboratory to clinical practice remains a challenge.[37] Part of the reason for the less-than-satisfactory results is the tendency to focus on isolated events in the ischemic cascades by modulating specific targets.[2] Thus, the discovery of pleiotropic, multi-target agents capable of regulating multiple pathways of pathological processes is crucial for effective neuroprotection.

As a characteristic component-based Chinese medicine, GXNT has been generally applied for treating cardiovascular diseases due to its multi-component and multi-target nature.[10] GXNT comprises two prominent "blood-invigorating and stasis-removing" Chinese herbs, Danshen and Chuanxiong. These herbs have been shown to exhibit a diverse range of pharmacological actions on the cardio-cerebrovascular system, including anti-atherosclerosis, anti-ischemia/reperfusion injury, neuroprotection, anti-inflammation, anti-apoptosis, anti-platelet aggregation, and oxidation resistance.[38–40] Correspondingly, beyond its established cardiovascular benefits, recent reports have revealed GXNT's potential for neuroprotection against conditions like Alzheimer's disease, diabetic encephalopathy, and acute CI/RI, achieved via the modulation of multiple pathways.[14–16] Based on these premises, we formulated a hypothesis that a multi-component medicine such as GXNT, targeting diverse molecular mechanisms, could potentially offer enhanced efficacy against post-

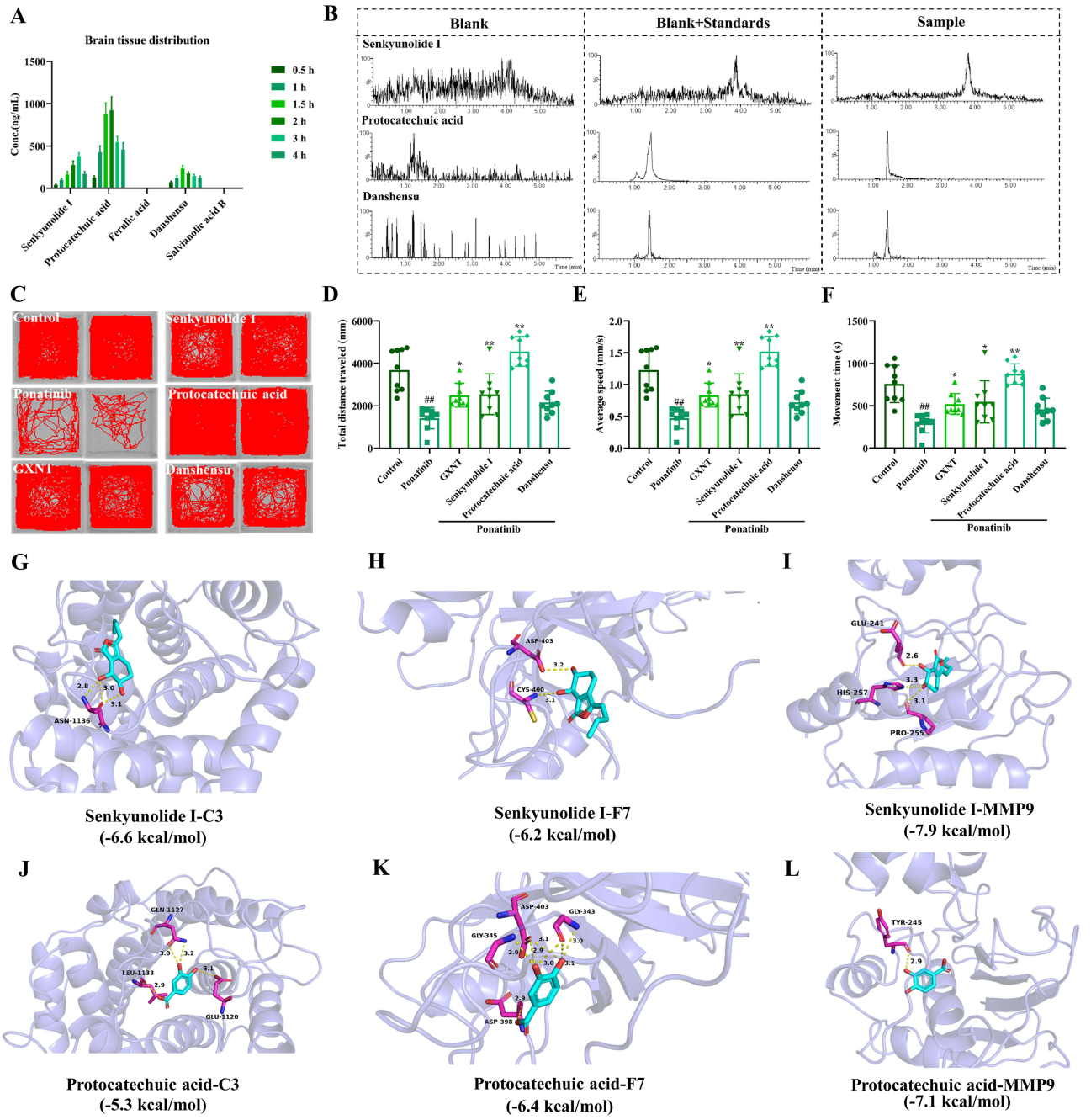

Figure 6 Discovery of anti-IS effective substances of GXNT. (**A**) The concentrations of different components in brain tissue at detection time points (n = 6). (**B**) The representative MRM chromatograms of brain tissue distribution of main ingredients in GXNT. (**C**) The representative images of motion tracking of zebrafish. Quantification of behavioral phenotypes of zebrafish (n = 9), including total swimming distance (**D**), average speed (**E**), and motion time (**F**). Compared with the ponatinib group without drug treatment, either senkyunolide I or protocatechuic acid intervention significantly improved the locomotor function of IS zebrafish. Molecular models of senkyunolide I binding to key proteins, including C3 (**G**), F7 (**H**), MMP9 (**I**). Molecular models of protocatechuic acid binding to key proteins, including C3 (**J**), F7 (**K**), MMP9 (**L**). Data are displayed as the mean ± SD. $^{\#\#}P < 0.01$ versus the control group; $^{*}P < 0.05$, and $^{**}P < 0.01$ versus the ponatinib group.

IS injury. This led to the question of identifying the potential functional pathways and anti-IS active substances within GXNT.

Under pathological conditions, ischemic brain injury triggers the production of various factors (eg reactive oxygen species, cytokines, chemokines, and vascular endothelial growth factor) in the ischemic brain tissue leading to BBB breakdown.[32,41] This, in turn, contributes to increased neutrophil infiltration, subsequently activating glial cells (microglia and astrocytes) through cytokines/chemokines release.[32,41] These interconnected cascades eventually cause post-IS

neuronal cell death and neurological deficits. Additionally, ischemic brain injury affects the motor cortices and their descending pathways, leading to post-IS motor deficits.[42] Encouragingly, this study unveiled, for the first time, the positive impacts of GXNT intervention in ameliorating neural and locomotor impairments in IS mice. Previously, the protective effects of GXNT against neuronal loss and BBB breakdown caused by diabetic encephalopathy have been reported.[16] As expected, the current work demonstrated the ability of GXNT to mitigate brain damage in the cortical regions and preserve BBB integrity (Figures 1 and 2), ultimately promoting the functional recovery after IS. These observed anti-IS effects of GXNT further supported its neuroprotective potential.

The growing body of evidence indicated the crucial involvement of the complement system, an essential part of innate immunity, in the pathogenesis of IS. Local accumulation of certain complement components in the post-IS brain tissue or the activation of complement system could elicit the inflammatory cascades and aggravate CI/RI.[43] Besides, the complement system takes a crucial role in neural plasticity and neurogenesis following IS.[43] Clinical reports have exhibited a positive correlation between elevated complement levels, particularly C3, in IS patients with worse neurological disability.[44,45] A pivotal process in IS involves the cleavage of prothrombin upon activation of the coagulation cascade.[46] Thrombin subsequently catalyzes the conversion of soluble fibrinogen into insoluble fibrin to form thrombi.[47] Elevated brain thrombin levels have been detected in the ischemic infarction area due to BBB disruption, prothrombin penetration and brain prothrombin synthesis. This can further compromise BBB integrity, trigger neuroinflammation, and exacerbate brain damage.[46,48,49] Currently, the interaction between the complement and coagulation systems is well established.[50] Notably, the complement system can enhance tissue factor activity, initiate the activation of extrinsic coagulation pathway, and generate activated thrombin.[33] Similarly, coagulation can induce the activity of complement factors as well.[51]

In our study, bioinformatics analysis based on RNA-seq emphasized the importance of complement and coagulation cascades pathway in GXNT's anti-IS effects (Figure 3). C3, a central constituent of the complement system-mediated inflammatory response in IS, offers neuroprotection via regulating the anaphylatoxin C3a-dependent mechanism.[52] F7, a crucial coagulation protease, initiates a cascade of proteolytic events culminating in thrombin production, fibrin deposition, and platelet activation.[53] Remarkably, C3 and F7 emerged as vital DEGs enriched in the complement and coagulation cascades pathway (Figure 4A and B), which were further verified via normalized mRNA and protein levels of C3 and F7 in the impaired cortical samples of tMCAO mice with GXNT treatment (Figure 4C-G). Additionally, GXNT treatment effectively modulated the transcriptional levels of other essential genes (Vwf, Thbd, Serpine1, F10, Procr, Serping1, and Tfpi) within the complement and coagulation cascades pathway (Figure 4C). These results revealed the close relationship between GXNT's anti-IS effects and its regulatory role in the complement and coagulation cascades pathway.

Several studies have reported that the activation of complement and coagulation systems induced a complex inflammatory network after IS through the regulation of adhesion molecules, neutrophil chemotaxis, platelet activation, and release of pro-inflammatory cytokines.[51,54] MMP3 and MMP9, key members of the matrix metalloproteinases family, have been implicated in BBB disruption, leukocyte infiltration, and progressive inflammatory reactions linked to IS.[55] In the current work, GXNT intervention substantially decreased both the mRNA and protein expression of MMP3 and MMP9 in comparison to the tMCAO group (Figure 5D,F-J). In addition, GXNT intervention effectively modulated the mRNA levels of other pro-inflammatory mediators, encompassing matrix metalloproteases (Mmp2, Mmp14), adhesion molecules (Icam1, Selp), chemokines (Cxcl1, Cxcl12, Cxcl13, Ccl7, Ccr1, Ccr2, Cxcr2, Cxcr4), and Tnfrsf1a (Figure 5D and E), and reduced TNF-α and IL-6 contents in cortical samples of tMCAO mice (Figure 5K and L). Collectively, these findings underscore GXNT's anti-inflammatory potential in response to post-IS injury, aligning with prior reports.[15]

To further discover the pharmacodynamic basis of GXNT's efficacy against post-IS injury, we first conducted investigations into brain tissue distribution. Interestingly, after oral administration of GXNT, senkyunolide I, protocatechuic acid, and danshensu were observed to rapidly enter the brain (Figure 6A and B), which were consistent with reports elsewhere.[56,57] Notably, these compounds have been previously linked to neuroprotective effect against CI/RI, suggesting their potential as anti-IS agents.[58–60] Then, we further displayed endogenous evidence of anti-IS activities of senkyunolide I and protocatechuic acid against behavioral disorders in ponatinib-induced zebrafish model of IS, although danshensu failed to positively regulate locomotor activity in IS zebrafish (Figure 6C-F). Based on the reported regulatory roles of senkyunolide I in coagulation cascade and neuroinflammation,[11,61] subsequent docking results supported direct binding between active compounds (senkyunolide I, protocatechuic acid) and key target proteins (C3, F7, MMP9)

(Figure 6G-L). These important findings first provided strong evidence suggesting senkyunolide I and protocatechuic acid as potential anti-IS active compounds within GXNT.

Finally, although this study elucidated GXNT's efficacy, potential functional mechanisms, and active compounds against post-IS injury, certain limitations warrant acknowledgement. First, further evaluation of GXNT's clinical impact on post-IS functional recovery is warranted. Second, casual-effect relationship between GXNT's anti-IS efficacy and its regulation on the complement and coagulation cascades and inflammatory network is still lacking. Third, the anti-IS activities of senkyunolide I and protocatechuic acid and their direct action targets merit further verification.

Conclusion

In conclusion, the present study provides a compelling evidence for GXNT's positive impacts on post-IS functional recovery, reduction of brain lesions, and mitigation of BBB disruption. These effects are potentially linked to the modulation of complement and coagulation cascades pathway and the orchestration of inflammatory network. Brain tissue distribution analysis highlighted the potential of senkyunolide I and protocatechuic acid as anti-IS compounds, demonstrated through behavioral improvements in a zebrafish model of IS and molecular docking interactions with key target proteins (C3, F7, MMP9). Collectively, these findings will enhance our understanding of GXNT's neuroprotective potential and provide a dependable reference for expanding GXNT's clinical applications. The discovery of these anti-IS active compounds holds the promise of novel drug development for IS treatment.

Abbreviations

ANOVA, one-way analysis of variance; BBB, blood–brain barrier; C3, complement component 3; CI/RI, cerebral ischemia/reperfusion injury; DAVID, Database for Annotation, Visualization and Integration Discovery; DEGs, differentially expressed genes; DMSO, Dimethyl sulfoxide; EB, Evans Blue; ELISA, Enzyme-Linked Immunosorbent Assay; F7, coagulation factor VII; GAPDH, glyceraldehyde 3-phosphate dehydrogenase; GO, Gene Ontology; GXNT, Guanxinning tablet; H&E, hematoxylin & eosin; IL-6, interleukin-6; IS, ischemic stroke; KEGG, Kyoto Encyclopedia of Genes and Genomes; MCC, maximal clique centrality; MMP3, matrix metallopeptidase 3; MMP9, matrix metallopeptidase 9; mNSS, modified Neurological Severity Score; MRM, multiple reaction monitoring; PDB, Protein Data Bank; PPI, protein–protein interaction; RT-qPCR, real-time quantitative polymerase chain reaction; STRING, Search Tool for Recurring Instances of Neighboring Genes; tMCAO, Transient middle cerebral artery occlusion; TNF-α, tumor necrosis factor-α; TTC, 2, 3, 5-Triphenyl-2H-Tetrazolium Chloride; TUNEL, Terminal deoxynucleotidyl transferase dUTP nick end labeling.

Funding

This work was financially supported by grants from the National Natural Science Foundation of China (Grant No. 82104351), the Zhejiang Province Traditional Chinese Medicine Science and Technology Project (Grant No. 2024ZF023), the Zhejiang Provincial Natural Science Foundation of China (Grant No. LTGY23H290005), the Construction Fund of Key Medical Disciplines of Hangzhou (Grant No. OO20200055), and the Fundamental Research Funds for the Central Universities (Grant No. 226-2023-00114). We thank Jingyao Chen and Qiong Huang from the Core Facilities, Zhejiang University School of Medicine for technical support in histopathology experiments. We appreciate Shanghai Applied Protein Technology Co., Ltd. (Shanghai, China) for the technical support of transcriptome sequencing.

Disclosure

The authors have no conflict of interest to declare.

References

1. Tsao CW, Aday AW, Almarzooq ZI, et al. Heart disease and stroke statistics-2022 update: a report from the American heart association. *Circulation*. 2022;145(8):e153–e639. doi:10.1161/CIR.0000000000001052

2. Paul S, Candelario-Jalil E. Emerging neuroprotective strategies for the treatment of ischemic stroke: an overview of clinical and preclinical studies. *Exp Neurol*. 2021;335:113518. doi:10.1016/j.expneurol.2020.113518
3. Mendelson SJ, Prabhakaran S. Diagnosis and management of transient ischemic attack and acute ischemic stroke: a review. *JAMA*. 2021;325 (11):1088–1098. doi:10.1001/jama.2020.26867
4. Bhaskar S, Stanwell P, Cordato D, et al. Reperfusion therapy in acute ischemic stroke: dawn of a new era. *BMC Neurol*. 2018;18(1):8. doi:10.1186/s12883-017-1007-y
5. Su CY, Ming QL, Rahman K, et al. Salvia miltiorrhiza: traditional medicinal uses, chemistry, and pharmacology. *Chin J Nat Med*. 2015;13 (3):163–182. doi:10.1016/S1875-5364(15)30002-9
6. Chen Z, Zhang C, Gao F, et al. A systematic review on the rhizome of Ligusticum chuanxiong Hort. *Food Chem Toxicol*. 2018;119:309–325. doi:10.1016/j.fct.2018.02.050
7. Wang ML, Yang QQ, Ying XH, et al. Network pharmacology-based approach uncovers the mechanism of GuanXinNing tablet for treating thrombus by MAPKs signal pathway. *Front Pharmacol*. 2020;11:652. doi:10.3389/fphar.2020.00652
8. Sun MY, Miao Y, Jin M, et al. Effect and safety of Guanxinning tablet for stable angina pectoris patients with Xin (Heart)-blood stagnation syndrome: a randomized, multicenter, placebo-controlled trial. *Chin J Integr Med*. 2019;25(9):684–690. doi:10.1007/s11655-019-3069-8
9. Zi M, Li R, Lu F, et al. Clinical study for safety evaluation of GXN tablets combined with aspirin in long-term treatment of coronary heart disease. *Evid Based Complement Alternat Med*. 2021;2021:6658704. doi:10.1155/2021/6658704
10. Cheng YY, Wang Y, Liu L, et al. Theoretical innovation of component-based Chinese medicine and its exemplary practice: the study on creating Guanxinning tablets. *Zhongguo Zhong Yao Za Zhi*. 2022;47(17):4545–4550. Chinese. doi:10.19540/j.cnki.cjcmm.20220804.301
11. Li J, Liu H, Yang Z, et al. Synergistic effects of cryptotanshinone and senkyunolide I in Guanxinning tablet against endogenous thrombus formation in zebrafish. *Front Pharmacol*. 2021;11:622787. doi:10.3389/fphar.2020.622787
12. Yang Q, Xu Y, Shen L, et al. Guanxinning tablet attenuates coronary atherosclerosis via regulating the gut microbiota and their metabolites in Tibetan minipigs induced by a high-fat diet. *J Immunol Res*. 2022;2022:7128230. doi:10.1155/2022/7128230
13. Ling Y, Shi J, Ma Q, et al. Vasodilatory effect of Guanxinning tablet on rabbit thoracic aorta is modulated by both endothelium-dependent and -independent mechanism. *Front Pharmacol*. 2021;12:754527. doi:10.3389/fphar.2021.754527
14. Zhang F, Xu Y, Shen L, et al. GuanXinNing tablet attenuates Alzheimer's disease via improving gut microbiota, host metabolites, and neuronal apoptosis in rabbits. *Evid Based Complement Alternat Med*. 2021;2021:9253281. doi:10.1155/2021/9253281
15. Hui XR, Jin Q, He JM, et al. Mechanism of Guanxinning against cerebral ischemia-reperfusion injury in mice based on transcriptomic analysis. *Zhongguo Zhong Yao Za Zhi*. 2022;47(11):3015–3022. Chinese. doi:10.19540/j.cnki.cjcmm.20220322.402
16. Li Y, Chen J, Tu H, et al. Protective effects of GuanXinNing tablet (GXNT) on diabetic encephalopathy in Zucker diabetic obesity (ZDF) rats. *BMC Complement Med Ther*. 2023;23(1):385. doi:10.1186/s12906-023-04195-2
17. Chen J, Wang Y, Wang S, et al. Salvianolic acid B and ferulic acid synergistically promote angiogenesis in HUVECs and zebrafish via regulating VEGF signaling. *J Ethnopharmacol*. 2022;283:114667. doi:10.1016/j.jep.2021.114667
18. Wang Y, He S, Liu X, et al. Galectin-3 mediated inflammatory response contributes to neurological recovery by QiShenYiQi in subacute stroke model. *Front Pharmacol*. 2021;12:588587. doi:10.3389/fphar.2021.588587
19. Wang Y, Liu X, Zhang W, et al. Synergy of "Yiqi" and "Huoxue" components of QishenYiqi formula in ischemic stroke protection via lysosomal/inflammatory mechanisms. *J Ethnopharmacol*. 2022;293:115301. doi:10.1016/j.jep.2022.115301
20. Wang Y, Wu H, Han Z, et al. Guhong injection promotes post-stroke functional recovery via attenuating cortical inflammation and apoptosis in subacute stage of ischemic stroke. *Phytomedicine*. 2022;99:154034. doi:10.1016/j.phymed.2022.154034
21. Wang Y, Wu H, Sheng H, et al. Discovery of anti-stroke active substances in Guhong injection based on multi-phenotypic screening of zebrafish. *Biomed Pharmacother*. 2022;155:113744. doi:10.1016/j.biopha.2022.113744
22. Frechou M, Margaill I, Marchand-Leroux C, et al. Behavioral tests that reveal long-term deficits after permanent focal cerebral ischemia in mouse. *Behav Brain Res*. 2019;360:69–80. doi:10.1016/j.bbr.2018.11.040
23. Weber RZ, Mulders G, Kaiser J, et al. Deep learning-based behavioral profiling of rodent stroke recovery. *BMC Biol*. 2022;20(1):232. doi:10.1186/s12915-022-01434-9
24. Hatfield RH, Mendelow AD, Perry RH, et al. Triphenyltetrazolium chloride (TTC) as a marker for ischaemic changes in rat brain following permanent middle cerebral artery occlusion. *Neuropathol Appl Neurobiol*. 1991;17(1):61–67. doi:10.1111/j.1365-2990.1991.tb00694.x
25. Wang Y, Xiao G, He S, et al. Protection against acute cerebral ischemia/reperfusion injury by QiShenYiQi via neuroinflammatory network mobilization. *Biomed Pharmacother*. 2020;125:109945. doi:10.1016/j.biopha.2020.109945
26. Xiao G, Lyu M, Li Z, et al. Restoration of early deficiency of axonal guidance signaling by guanxinning injection as a novel therapeutic option for acute ischemic stroke. *Pharmacol Res*. 2021;165:105460. doi:10.1016/j.phrs.2021.105460
27. Loo DT. In situ detection of apoptosis by the TUNEL assay: an overview of techniques. *Methods Mol Biol*. 2011;682:3–13. doi:10.1007/978-1-60327-409-8_1
28. Dennis G, Sherman BT, Hosack DA, et al. DAVID: database for annotation, visualization, and integrated discovery. *Genome Biol*. 2003;4(5):P3. doi:10.1186/gb-2003-4-5-p3
29. Chin CH, Chen SH, Wu HH, et al. cytoHubba: identifying hub objects and sub-networks from complex interactome. *BMC Syst Biol*. 2014;8(Suppl 4(Suppl 4)):S11. doi:10.1186/1752-0509-8-S4-S11
30. Zhu XY, Xia B, Ye T, et al. Ponatinib-induced ischemic stroke in larval zebrafish for drug screening. *Eur J Pharmacol*. 2020;889:173292. doi:10.1016/j.ejphar.2020.173292
31. Kadian N, Raju KS, Rashid M, et al. Comparative assessment of bioanalytical method validation guidelines for pharmaceutical industry. *J Pharm Biomed Anal*. 2016;126:83–97. doi:10.1016/j.jpba.2016.03.052
32. Jiang X, Andjelkovic AV, Zhu L, et al. Blood-brain barrier dysfunction and recovery after ischemic stroke. *Prog Neurobiol*. 2018;163:144–171. doi:10.1016/j.pneurobio.2017.10.001
33. Berkowitz S, Chapman J, Dori A, et al. Complement and coagulation system crosstalk in synaptic and neural conduction in the central and peripheral nervous systems. *Biomedicines*. 2021;9(12):1950. doi:10.3390/biomedicines9121950
34. Zou Y, Gong P, Zhao W, et al. Quantitative iTRAQ-based proteomic analysis of piperine protected cerebral ischemia/reperfusion injury in rat brain. *Neurochem Int*. 2019;124:51–61. doi:10.1016/j.neuint.2018.12.010

35. Lambertsen KL, Finsen B, Clausen BH. Post-stroke inflammation-target or tool for therapy. *Acta Neuropathol*. 2019;137(5):693–714. doi:10.1007/s00401-018-1930-z
36. Neil HP. Stroke Rehabilitation. *Crit Care Nurs Clin North Am*. 2023;35(1):95–99. doi:10.1016/j.cnc.2022.11.002
37. Haupt M, Gerner ST, Bahr M, et al. Neuroprotective strategies for ischemic stroke-future perspectives. *Int J Mol Sci*. 2023;24(5):4334. doi:10.3390/ijms24054334
38. Li ZM, Xu SW, Liu PQ. Salvia miltiorrhizaBurge (Danshen): a golden herbal medicine in cardiovascular therapeutics. *Acta Pharmacol Sin*. 2018;39(5):802–824. doi:10.1038/aps.2017.193
39. Li D, Long Y, Yu S, et al. Research advances in cardio-cerebrovascular diseases of Ligusticum chuanxiong hort. *Front Pharmacol*. 2022;12:832673. doi:10.3389/fphar.2021.832673
40. Jiang HJ, Huang XL, Xian B, et al. Chinese herbal injection for cardio-cerebrovascular disease: overview and challenges. *Front Pharmacol*. 2023;14:1038906. doi:10.3389/fphar.2023.1038906
41. Yang C, Hawkins KE, Dore S, et al. Neuroinflammatory mechanisms of blood-brain barrier damage in ischemic stroke. *Am J Physiol Cell Physiol*. 2019;316(2):C135–C153. doi:10.1152/ajpcell.00136.2018
42. Hosp JA, Luft AR. Cortical plasticity during motor learning and recovery after ischemic stroke. *Neural Plast*. 2011;2011:871296. doi:10.1155/2011/871296
43. Ma Y, Liu Y, Zhang Z, et al. Significance of complement system in ischemic stroke: a comprehensive review. *Aging Dis*. 2019;10(2):429–462. doi:10.14336/AD.2019.0119
44. Cojocaru IM, Cojocaru M, Tanasescu R, et al. Changes in plasma levels of complement in patients with acute ischemic stroke. *Rom J Intern Med*. 2008;46(1):77–80.
45. Yang P, Zhu Z, Zang Y, et al. Increased serum complement C3 levels are associated with adverse clinical outcomes after ischemic stroke. *Stroke*. 2021;52(3):868–877. doi:10.1161/STROKEAHA.120.031715
46. Ye F, Garton HJL, Hua Y, et al. The role of thrombin in brain injury after hemorrhagic and ischemic stroke. *Translational Stroke Research*. 2021;12(3):496–511. doi:10.1007/s12975-020-00855-4
47. Pan L, Peng C, Wang L, et al. Network pharmacology and experimental validation-based approach to understand the effect and mechanism of Taohong Siwu decoction against ischemic stroke. *J Ethnopharmacol*. 2022;294:115339. doi:10.1016/j.jep.2022.115339
48. Bushi D, Chapman J, Katzav A, et al. Quantitative detection of thrombin activity in an ischemic stroke model. *J Mol Neurosci*. 2013;51(3):844–850. doi:10.1007/s12031-013-0072-y
49. Shavit-Stein E, Berkowitz S, Gofrit SG, et al. Neurocoagulation from a mechanistic point of view in the central nervous system. *Semin Thromb Hemost*. 2022;48(3):277–287. doi:10.1055/s-0041-1741569
50. Amara U, Rittirsch D, Flierl M, et al. Interaction between the coagulation and complement system. *Adv Exp Med Biol*. 2008;632:71–79. doi:10.1007/978-0-387-78952-1_6
51. Oikonomopoulou K, Ricklin D, Ward PA, et al. Interactions between coagulation and complement--their role in inflammation. *Semin Immunopathol*. 2012;34(1):151–165. doi:10.1007/s00281-011-0280-x
52. Mocco J, Mack WJ, Ducruet AF, et al. Complement component C3 mediates inflammatory injury following focal cerebral ischemia. *Circ Res*. 2006;99(2):209–217. doi:10.1161/01.RES.0000232544.90675.42
53. Eigenbrot C. Structure, function, and activation of coagulation factor VII. *Curr Protein Pept Sci*. 2002;3(3):287–299. doi:10.2174/1389203023380675
54. Rawish E, Sauter M, Sauter R, et al. Complement, inflammation and thrombosis. *Br J Pharmacol*. 2021;178(14):2892–2904. doi:10.1111/bph.15476
55. Yang Y, Rosenberg GA. Matrix metalloproteinases as therapeutic targets for stroke. *Brain Res*. 2015;1623:30–38. doi:10.1016/j.brainres.2015.04.024
56. He CY, Wang S, Feng Y, et al. Pharmacokinetics, tissue distribution and metabolism of senkyunolide I, a major bioactive component in Ligusticum chuanxiong hort. *J Ethnopharmacol*. 2012;142(3):706–713. doi:10.1016/j.jep.2012.05.047
57. Zhang YJ, Wu L, Zhang QL, et al. Pharmacokinetics of phenolic compounds of Danshen extract in rat blood and brain by microdialysis sampling. *J Ethnopharmacol*. 2011;136(1):129–136. doi:10.1016/j.jep.2011.04.023
58. Hu Y, Duan M, Liang S, et al. Senkyunolide I protects rat brain against focal cerebral ischemia-reperfusion injury by up-regulating p-Erk1/2, Nrf2/HO-1 and inhibiting caspase 3. *Brain Res*. 2015;1605:39–48. doi:10.1016/j.brainres.2015.02.015
59. Gao Q, Deng H, Yang Z, et al. Sodium danshensu attenuates cerebral ischemia-reperfusion injury by targeting AKT1. *Front Pharmacol*. 2022;13:946668. doi:10.3389/fphar.2022.946668
60. Kale S, Sarode LP, Kharat A, et al. Protocatechuic acid prevents early hour ischemic reperfusion brain damage by restoring imbalance of neuronal cell death and survival proteins. *J Stroke Cerebrovasc Dis*. 2021;30(2):105507. doi:10.1016/j.jstrokecerebrovasdis.2020.105507
61. Hu YY, Wang Y, Liang S, et al. Senkyunolide I attenuates oxygen-glucose deprivation/reoxygenation-induced inflammation in microglial cells. *Brain Res*. 2016;1649(Pt A):123–131. doi:10.1016/j.brainres.2016.08.012